CHEMISTRY
A European Journal

A Journal of
ChemPubSoc Europe

Accepted Article

Title: Efficient catalytic microreactors with atomic layer deposited platinum nanoparticles on oxide support

Authors: Ville Rontu, Anne Selent, Vladimir Zhivonitko, Gianmario Scotti, Igor Koptyug, Ville-Veikko Telkki, and Sami Franssila

To be cited as: *Chem. Eur. J.* 10.1002/chem.201703391

Link to VoR: http://dx.doi.org/10.1002/chem.201703391

Supported by
ACES

WILEY-VCH

10.1002/chem.201703391

Efficient catalytic microreactors with atomic layer deposited platinum nanoparticles on oxide support

Ville Rontu†*[a], A. Selent†[b], Vladimir V. Zhivonitko[b,c,d], Gianmario Scotti[a], Igor V. Koptyug[c,d], Ville-Veikko Telkki[b] and Sami Franssila[a]

a. V. Rontu, Dr. G. Scotti, Prof. Dr. S. Franssila
Department of Chemistry and Materials Science
Aalto University
P.O. Box 16200, 00076 Aalto, Finland
E-mail: ville.rontu@aalto.fi

b. A. Selent, Dr. V. V. Zhivonitko, Dr. V.-V. Telkki
NMR Research Unit
University of Oulu
P.O.Box 3000, 90014 University of Oulu, Finland

c. Dr. V. V. Zhivonitko, Prof. Dr. I. V. Koptyug
Laboratory of Magnetic Resonance Microimaging
International Tomography Center SB RAS
3A Institutskaya St., Novosibirsk 630090, Russia

d. Dr. V. V. Zhivonitko, Prof. Dr. I. V. Koptyug
Novosibirsk State University
Pirogova St. 2, Novosibirsk 630090, Russia

†These authors contributed equally to the work.

Supporting information for this article is available on the WWW under
http://dx.doi.org/10.1002/chem.2017xxxxx

Abstract

Microreactors attract a significant interest for chemical synthesis due to benefits of small scales such as high surface to volume ratio, rapid thermal ramping and well-understood laminar flows. The suitability of atomic layer deposition for applying of both the catalyst nanoparticles and the support material on the surfaces of channels of microfabricated silicon microreactors is demonstrated in this research. Continuous flow hydrogenation of propene into propane at low temperatures with TiO_2 supported catalytic Pt nanoparticles was used as a model reaction. Reaction yield and mass transport were monitored by high sensitivity microcoil Nuclear Magnetic Resonance (NMR) spectroscopy as well as time-of-flight remote detection NMR imaging. The microreactors were shown to be very efficient in propene conversion into propane. The yield of 100 % was achieved at 50 °C with a reactor decorated with Pt nanoparticles of average size of ca. 1 nm and surface coverage of 3.2 % in 20 mm long reaction channels with the residence time of 1100 ms. The activity of the Pt catalyst surfaces was on the order of few to tens of mmol $s^{-1}m^{-2}$.

10.1002/chem.201703391

Introduction

Catalysts are used in the majority of industrial chemical processes. Demand for sustainable operation requires efficient use of noble metal catalysts and waste minimization. There is still room for improvement even in well-established processes such as hydrogenation in terms of catalytic activity, selectivity and stability.[1,2] Small dimensions have been shown to result in the enhanced properties which might promote better catalytic activity.[3,4]

Microreactors have attracted interest for chemical synthesis due to the benefits that small dimensions bring in terms of heat and mass transport, hydrodynamics, low reactant consumption and safety of operation.[5,6] Development of flow chemistry and stable catalysts would enable microreactors to be operated continuously. The production could be scaled-up by numbering up the microreactors instead of scaling up the batch volumes, which enables optimization of process parameters already at the laboratory scale.[5] Silicon microfabrication techniques allow easy fabrication of microfluidic channels and could be used to fabricate the microreactors as they are well-established and suitable for mass production.

In wall-coated microreactors, catalyst is deposited on the walls of the microchannels. This reduces the active surface area of the catalyst compared to packed microchannels, but eases the flow through the channels. An intermediate alternative could be a semipacked microreactor with e.g. lithographically defined pillars. Efficient mass transport in small channels enables, however, high yields even with wall-coated catalysts.

Atomic layer deposition (ALD) has been used to create various supports, catalysts and overcoats for heterogeneous catalysis.[7] It is based on self-limiting surface reactions from sequential precursor pulses of two or more different precursors that are separated from each other typically by inert gas purging.[8,9] Advantage of ALD is the ability to deposit controllably very thin conformal layers stemming from the self-limiting surface reactions and separation of precursor pulses.[10] In addition to depositing layered materials, ALD can be used to deposit metal nanoparticles such as Pt on oxide surfaces by exploiting distinctive nucleation behavior. Metal ALD initiates as nanoparticles on oxide surfaces, because metals do not wet the oxide surface due to large difference in surface energies, and forms a continuous layer only once the nanoparticles coalesce.[11,12] Main focus in applying ALD to catalysis has been to coat high-surface area materials such as carbon black[13,14] and various other powders.[15–17] However, it is difficult to achieve true growth saturation during a deposition cycle due to long pulse and purge times required with high-surface area materials, and thus the accuracy and control of nanoscale catalyst design is compromised. In addition, all of the methods developed for catalyst design by ALD are not applicable to powders, such as

plasma-enhanced atomic layer deposition (PEALD). On the other hand, they can be applied to deposit catalysts on the channel walls.

Deposition of catalyst material directly into a microreactor by ALD was demonstrated by Karinen et al.[18] by depositing ALD chromia catalyst to alumina support. However, ALD, so far, has not been applied to deposit metallic catalyst nanoparticles directly into microreactors. In this work, we fabricate wall-coated silicon microreactors where both TiO_2 catalyst support and Pt catalyst nanoparticles are deposited by ALD. We use these microreactors in hydrogenation of propene to propane at low (close to room) temperatures.

Microfluidic processes are traditionally monitored either by optical,[19,20] electrochemical[21] or mass spectrometry[22] methods. Among these, optical and electrochemical methods are the most frequently used due to their high sensitivity.[23,24] Nuclear Magnetic Resonance (NMR) spectroscopy is another powerful method to characterize microfluidic devices.[25,26] It is a non-invasive method to obtain versatile spatial, spectral and dynamic information from a microfluidic device without the need for optical transparency or additional tracer molecules. The weak spot of NMR is its low sensitivity, being emphasized in the microfluidic devices with small channels and low filling factors. The sensitivity problem is especially difficult when low density gaseous fluids are investigated. However, the sensitivity can be improved by several orders of magnitude using ultrasensitive miniaturized coil designs, such as microsolenoids,[27] planar surface coils or microcoils,[28–32] microstriplines and microslots,[33–35] or by increasing nuclear spin polarization degree exploiting hyperpolarization methods, such as spin-exchange optical pumping (SEOP) or parahydrogen-induced polarization (PHIP) techniques.[36–42]

In this work, the yield of the hydrogenation reaction in the microfluidic chips was determined from ^{1}H NMR spectra measured by an ultrasensitive microsolenoid wound around an outlet capillary, while the gas mixture was flowing out from the reactor. Furthermore, Remote Detection (RD) NMR[43,44] was utilized for visualization of the gas flow in the reactors. In RD NMR imaging, the spatial information is encoded in spin coherences by a large radio frequency (RF) coil surrounding the microfluidic reactor and the detection is performed with the ultrasensitive microsolenoid around the outlet tubing (see Figure 1). RD has been shown to provide an 800-fold sensitivity boost as compared to a corresponding experiment carried out by the large coil around the reactor.[45] The method provides also time-of-flight (TOF) information as the travel time from the encoding region to the detector depends on the initial spatial position of the encoded molecule. Therefore, RD NMR is an ideal tool for TOF flow imaging in microfluidic devices.[36,46,47] Recently, we have demonstrated that the high sensitivity of RD NMR can also be exploited in imaging of gas phase

chemical reactions inside microfluidic devices.[39,45,48] Now the state-of-the-art NMR techniques are exploited in the characterization of novel, efficient, ALD coated microreactors.

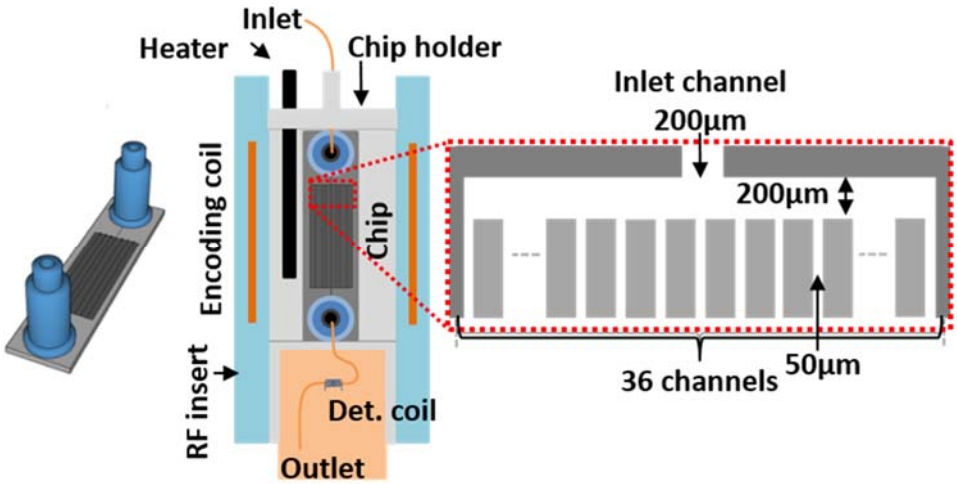

Figure 1. RD NMR experimental setup. The microfluidic chip was fixed in the center of the encoding coil by a chip holder, and the detection coil was wound around the outlet tubing.

Results and discussion

Microreactor fabrication

ALD processes are affected by the starting surface. Silicon surface is homogeneous and well-known, while the main alternative material for microreactors, steel, is not. This is why silicon is easier substrate than steel to work with when depositing catalysts by ALD. Microfabrication techniques are well-established by semiconductor industry and channel dimensions on silicon can be fabricated with few micrometer tolerances using photolithography and DRIE etching.

Channel depth was 100 µm for all microreactor chips studied in this work, except for PirSi 50c chips that were fabricated in a separate batch. The channel depth for these chips was 60 µm due to an unknown variation in etch rate in our cryogenic ICP-RIE.

Our novel capping method utilizing laminating foil allowed gas tight capping of the microreactors with inert film. The biggest advantage of this is that this capping method can be applied regardless of what is the opposite interface material and it is also insensitive to minor surface roughness. This allows easy fabrication of catalytic microreactors for low temperature experiments. The temperature tolerance can be increased slightly by using more temperature tolerant polymers.

10.1002/chem.201703391

Pt nanoparticle catalyst characterization

Pt nanoparticles were deposited by PEALD from trimethyl-(methylcyclopentadienyl)-platinum(IV) ($MeCpPtMe_3$) and O_2-plasma at 300 °C on Piranha treated silicon (PirSi) or on ALD TiO_2 surface. The catalyst loading was controlled with number of ALD cycles, one cycle consisting of $MeCpPtMe_3$ and O_2-plasma pulses and following purges. With growing number of ALD cycles, the particle size and the surface coverage of the Pt nanoparticles increased. This is clearly visible from Figure 2, where TEM images of Pt on TiO_2 with 10, 40 and 80 cycles of Pt are shown. The mean Pt particle size and the surface coverage on Si_3N_4 TEM windows after 5, 10, 20 and 40 cycles are shown in Table 1. The particles have already started to coalesce on the surface of the sample with 80 cycles. Some coalescence was observed also for Piranha treated sample with 50 cycles of Pt deposited. The apparent particle size on SEM images is slightly larger than from TEM images due to resolution limit of SEM.

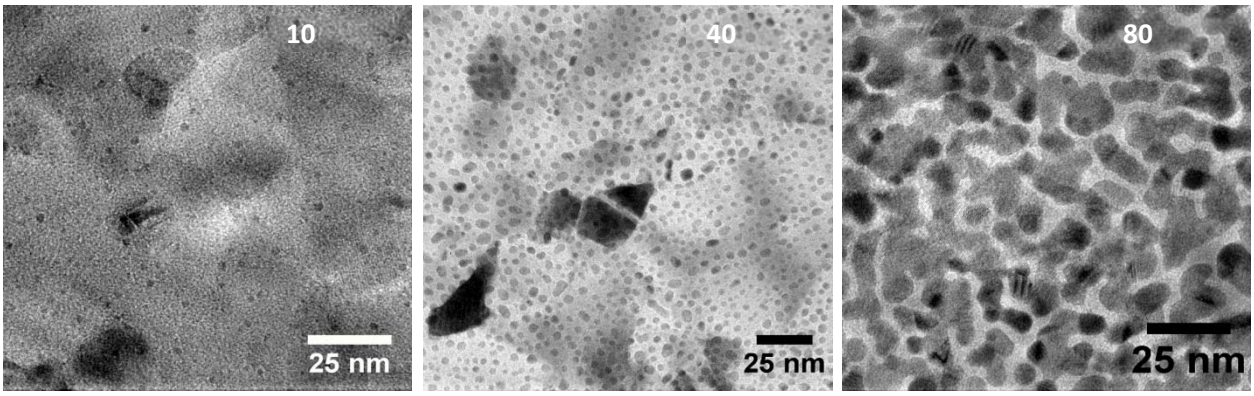

Figure 2. TEM images of Pt particles on top of 20 nm ALD TiO_2. The number of Pt deposition cycles: 10 (left), 40 (middle), and 80 (right). TiO_2 at 20 nm thickness is partly crystalline and some TiO_2 grains are visible.

Table 1. Mean particle size and surface coverage of Pt nanoparticles deposited on Si_3N_4 TEM windows with ALD TiO_2 support or Piranha treated silicon (PirSi) with different number of deposition cycles. Imaging of ALD TiO_2 support was done with TEM and PirSi support with SEM.

Starting surface	**Number of Pt ALD cycles**	**Mean particle size (nm)**	**Surface coverage, S_c (%)**
ALD TiO_2	5	0.8 ± 0.2	1.2
ALD TiO_2	10	0.9 ± 0.4	2.0
ALD TiO_2	20	1.1 ± 0.5	3.2
ALD TiO_2	40	2.8 ± 1.2	25
PirSi	40	3.7 ± 1.3	5.1
PirSi	50	-	46

10.1002/chem.201703391

Particle size distributions (Figure 3) show widening of the distribution with increasing number of ALD cycles. This means that new particles are formed continuously on the substrate surface. Widening of the particle size distribution has been observed also for thermal Pt processes using O_2 at 300 °C.[11] Narrow particle size distributions with controlled size are desired for catalysis purposes since catalytic activity can depend on the particle size.[1] To deposit catalyst particles with narrow particle size distribution, new means to avoid nucleation of new particles after first few cycles need to be developed. Recently, some novel methods to achieve this goal have been presented by Lu et al.[49] and Weber et al.[12,50] based on selective deposition on pre-existing nanoparticles and by Mackus et al.[11] based on low temperature three-step plasma process.

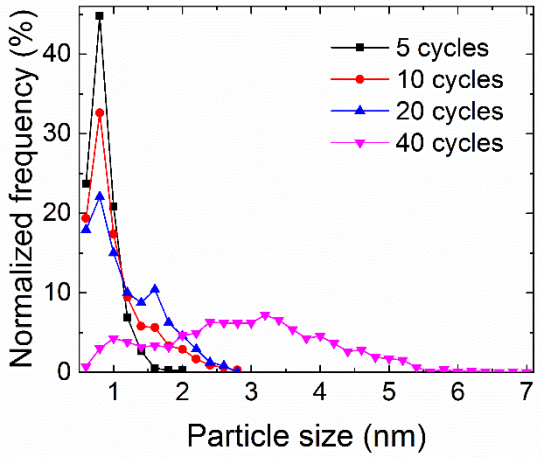

Figure 3. Particle size distributions for Pt particles deposited on top of TEM windows with TiO_2.

Lateral growth rate of Pt nanoparticles on TiO_2 was 0.09±0.04 nm/cycle based on the calculated average particle sizes. Our growth rate is twice as high as the rate observed by Mackus et al.[11] on ALD Al_2O_3 using thermal process with O_2 at 300 °C or O_2-plasma/H_2-plasma ABC process at room temperature. Comparing SEM images from Baker et al.[51] for Pt nucleation using O_2-plasma on ALD Al_2O_3 with results from Mackus et al.,[11] the nucleation using O_2-plasma appears to be faster.

Particle sizes on the TEM grids are assumed to correspond to the particle size on the microreactors as both are deposited on top of ALD TiO_2 even though TiO_2 on top of TEM grids is only partly crystallized whereas 50 nm of TiO_2 on surface of microreactors is expected to be fully crystalline. Assuming that the particles are hemispherical, active Pt surface area is twice the surface coverage of Pt on TEM or SEM images. Table 2 shows the active catalyst surface area in the microreactors. The surface area on PirSi 50c 20mm sample is an overestimate as most of the particles have already coalesced to form elongated Pt islands.

10.1002/chem.201703391

The amount of Pt deposited during one ALD cycle is dependent on the amount of $MeCpPtMe_3$ adsorbed on substrate surface. Initial adsorption occurs on hydroxyl groups[16] and is limited either by the number of available hydroxyl groups or by the steric hindrance of already adsorbed precursor molecules. Piranha treatment oxidizes silicon surface and leaves it hydroxyl terminated. Significantly lower Pt particle loading on microreactor with 40 ALD cycles on Piranha treated silicon surface (PirSi 40c) compared to 50 ALD cycles (PirSi 50c) (Figure 4) may be related to smaller hydroxyl group density on the surface due to difference in Piranha treatment of the silicon surface. There was no fresh H_2O_2 added to the Piranha solution in the tank at the stage when PirSi 40c microreactor was Piranha treated to prepare the support for Pt deposition, reducing the oxidizing strength of the solution. This may have led to number of the hydroxyl groups being the major limiting factor for the Pt deposition instead of steric hindrance. This goes to demonstrate how important the starting surface is for metal deposition by ALD.

*Table 2. Active Pt surface area for samples with different oxide support, number of Pt ALD cycles and channel length. Values for the reaction yield, reaction rate k and activity at the beginning of the flow for the non-heated and heated situation. *Overestimate as assumption of hemispherical particles is invalid due to particle coalescence. **Reaction conditions different from others in this work.*

Sample (support, number of Pt ALD cycles, channel length)	**Pt surface area, A_{Pt} (mm^2)**	**Contact time (ms)**	**Yield at 21 °C (%)**	***k* at 21 °C (s^{-1})**	**Activity of Pt surface at 21 °C, *A* (mmol $s^{-1}m^{-2}$)**	**Yield at 50 °C (%)**	***k* at 50 °C (s^{-1})**	**Activity of Pt surface at 50 °C, *A* (mmol $s^{-1}m^{-2}$)**	**Data from**
TiO_2, 40c, 20mm	96	1100 ± 150	90 ± 3	0.28 ± 0.05	2.0 ± 0.4	100	-	-	This work
TiO_2, 20c, 20mm	12	1100 ± 150	62 ± 2	0.19 ± 0.04	10.7 ± 2.2	100	-	-	This work
TiO_2, 10c, 20mm	8	1100 ± 150	21 ± 2	0.06 ± 0.02	5.3 ± 1.3	40 ± 2	0.12 ± 0.02	9.1 ± 2.0	This work
TiO_2, 20c, 10mm	7	550 ± 80	46 ± 1	0.29 ± 0.05	16.5 ± 3.7	93 ± 3	0.59 ± 0.03	30.8 ± 3.4	This work
TiO_2, 10c, 10mm	4	550 ± 80	10 ± 2	0.06 ± 0.02	6.1 ± 2.3	31 ± 2	0.19 ± 0.02	17.9 ± 2.4	This work
TiO_2, 5c, 10mm	3	550 ± 80	0	0.00	0.0	-	-	-	This work
PirSi, 50c, 20mm	123*	650 ± 120	46** ± 2	0.24** ± 0.06	1.1** ± 0.3	100**	-	-	This work
Sputtered, 5 mm	48	170 ± 50	11	0.22 ± 0.09	0.4 ± 0.2	50	1.00 ± 0.02	1.6 ± 0.2	[39]
Sputtered, 10 mm	82	230 ± 60				22	0.32 ± 0.01	0.5 ± 0.1	[39]
Sputtered, 20 mm	149	380 ± 100	28	0.25 ± 0.09	0.4 ± 0.2				[39]

10.1002/chem.201703391

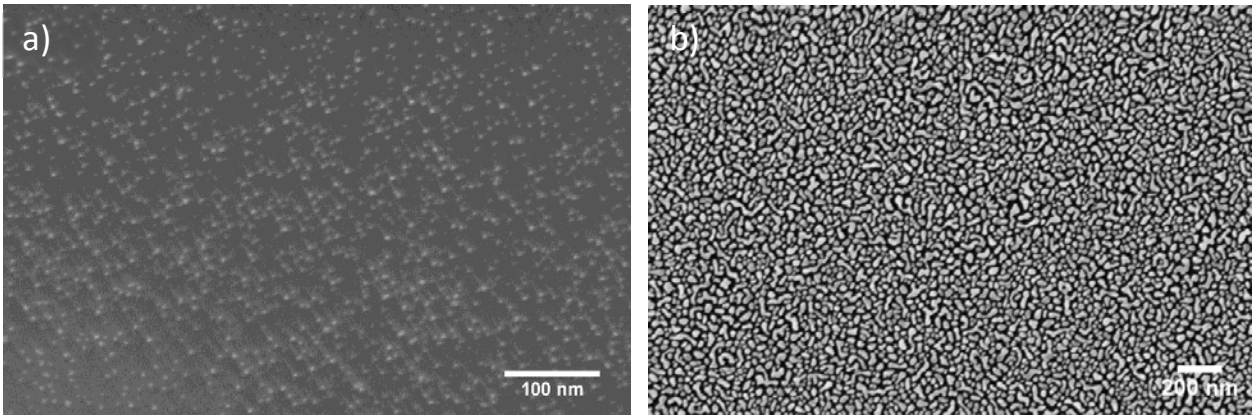

Figure 4. SEM image of Pt nanoparticles on Piranha treated silicon surface after 40 (a) and 50 ALD cycles (b).

NMR characterization

In order to investigate mass transport in the reactors, we measured 2D yz-encoded RD TOF NMR (see pulse sequence in Figure S3) images of flow of pure propene through a chip with 20 mm channel length. The images shown in Figure 5 reveal the initial position of the spins, which arrive to the detector at a certain time after the spatial encoding. Consequently, the spins at the exit (bottom) of the reactor are observed first and those at the entrance (top) last. The arrow-like shape of the images arises from the fact that the flow path through the outermost channels is longer than through the center channels. The arrow becomes slightly elongated at longer TOF instances, implying that the flow velocity is slightly smaller in the outermost channels than in the center. Small dispersion and regular shape of the pattern in the images indicate that the flow was similar in different channels, and variation in the channel dimensions was small. According to the TOF images, the travel time of the gas through the chip, which is equal to the contact time of gas with the catalyst, was about 1100 ms, while in the 10 mm reactor (TOF images not shown) it was about 550 ms. The flow velocity was the same in both reactors, 1.8 cm s^{-1}. For the 50 cycles Piranha treated chip with 20 mm channel length (60 μm channel depth) the travel time through the chip was about 650 ms. In the sum of all TOF images (in Figure 5 the right most panel), the signal amplitude is considerably higher in the lower part of the chip than in the upper part due to T_1 relaxation. T_1 of propene in the TiO_2 chip was determined from the image as explained in Ref. 45, and the resulting value was 600 ± 90 ms.

10.1002/chem.201703391

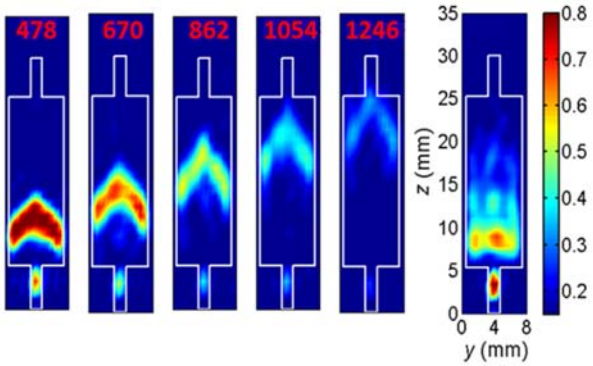

Figure 5. RD TOF NMR images of pure propene flowing through the chip with 20 mm channel length. The channels are outlined by white in the panels, and TOF in ms is shown on the top of the panels with red numbers. The image on the right-hand side shows all panels summed together.

The yield of the propene hydrogenation reaction in the chips was determined from the spectra measured by the detection coil around the outlet tubing, while the reaction gas mixture was continuously flowing through the reactor. The flow rate was kept constant in all the experiments, being the same as in the RD experiments above. The spectra for the chips with TiO_2 support are shown in Figure 6a. Although the linewidth in the spectra is relatively large (about 100 Hz) due to the short residence time of spins inside the detection coil (about 14 ms) and the effect of the magnetic susceptibility caused by the proximity of the coil wires (stopped flow linewidth was about 40 Hz), the spectral peaks of each component are well-resolved. Therefore, proportion of each component could be quantified based on peak integrals.

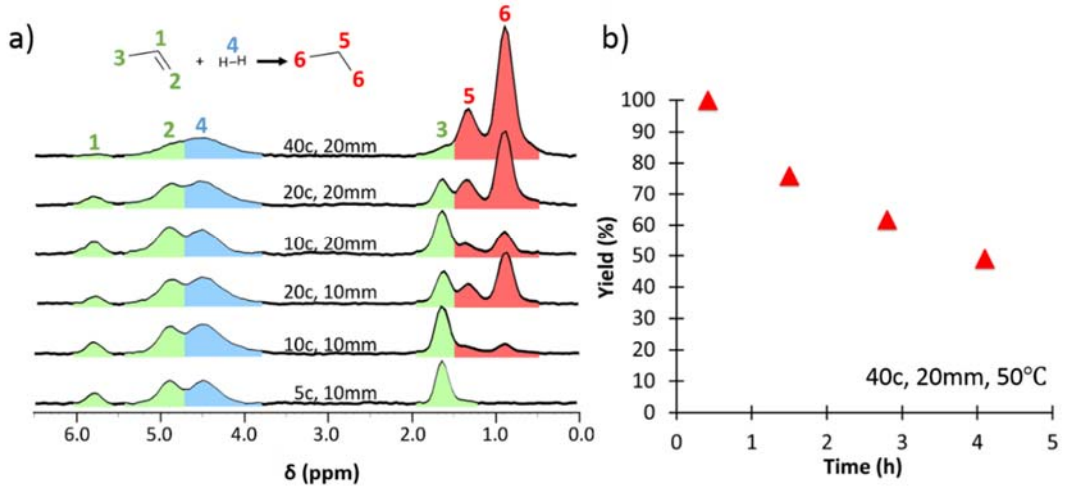

Figure 6. a) ^{1}H NMR spectra of the gas mixture flowing out from the reactor chips with TiO_2 support measured at room temperature, right after turning on the flow. The number of ALD cycles, length of reaction channels, as well as origin of the signals are indicated in the figure. b) Reaction yield, determined from ^{1}H spectra, as a function of time for the reactor with 20 mm channel length and 40 ALD cycles at 50 °C.

10.1002/chem.201703391

The resulting propane yields are shown in Table 2 and Figure 7. The reaction yield increases with increasing number of ALD cycles and channel length. At room temperature, the chip with 10 mm channels and 5 ALD cycles did not show any reaction product, but the yield for the chip with 20 mm channels and 40 ALD cycles was high, about 90 %. At 50 °C, the yield of 10 and 20 cycles chips was roughly double as compared to the room temperature experiments, and the chips with 20 mm channel length and 20 or 40 ALD cycles resulted in 100 % conversion. The reaction yields could be converted into reaction rate based on the first order kinetics (see Table 2 for results and Supporting Information for methods). The reaction rate, in turn, was converted into the activity of Pt surface (see Eq. 13 in Supporting Information). The activity was the highest for the 20 ALD cycles chips, 10.7–16.5 mmol $s^{-1}m^{-2}$ at room temperature and about 30.8 mmol $s^{-1}m^{-2}$ at 50 °C. This implies that the Pt nanoparticles with the size between 1 and 2 nm are the most active, because the 20 ALD cycles results in an unique peak on that region in the particle size distribution (see Figure 4), while the distributions of the 5 and 10 ALD cycles are centered around sizes below 1 nm and the 40 cycles distribution between 2-5 nm.

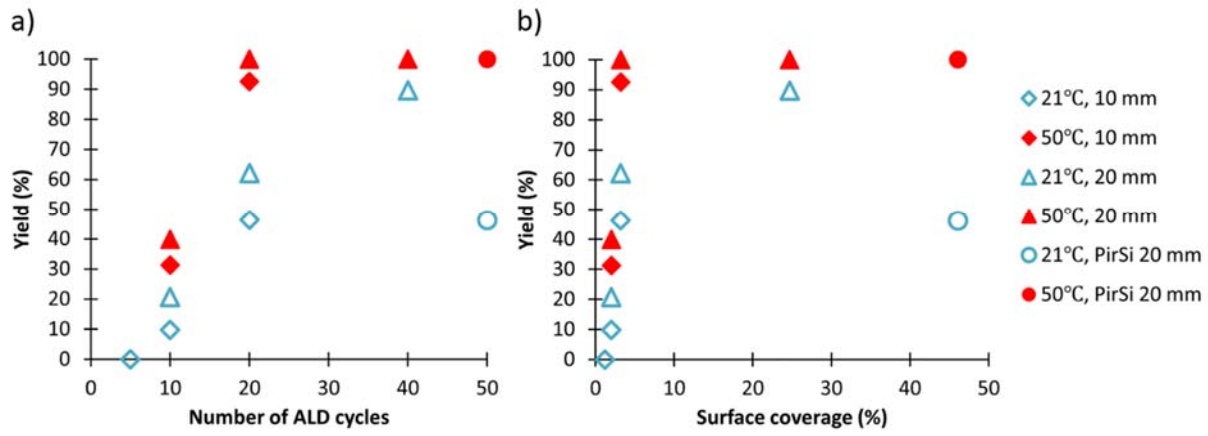

Figure 7. The reaction yield right after turning on the flow as a function of a) the number of ALD cycles and b) the Pt nanoparticles surface coverage. Results both at room temperature (indicated with blue hollow symbols) and at slightly elevated temperature (marked with red filled symbols) are shown. The TiO_2 reactors with 10 mm long channels are marked with diamond symbols, and the TiO_2 reactors with 20 mm long channels are marked with triangles. Piranha treated chip with 50 cycles of ALD is marked with circle. The measurement temperature and the length of the reaction channel is indicated in the labels.

Piranha treated chips with 40 ALD cycles of Pt did not show any yield whereas on TiO_2 10c 10 mm chip with smaller Pt nanoparticles (0.9 vs. 3.7 nm) and lower surface coverage (2.0 vs. 5.1 %) did show 10 % yield at 21 °C. The reasons for this are not very well understood, but probably concern the influence of the support nature as experimental conditions were quite similar for these chips.[52] On the other hand, PirSi 50c chip showed 46 % yield at 21 °C and 100 % yield at 50 °C, likely due to the much higher surface

coverage (46 vs. 5.1 %, Table 1 and Figure 7b). The results of the PirSi 50c chip and TiO_2 chips shown in Table 2 and Figure 7 are not, however, fully comparable because of the smaller channel depth in the former chips (see Microreactor fabrication section) and slightly different experimental conditions (propene:H_2 ratio was higher, 2:3, total gas pressure was higher, 7.5 bar, gas residence time in the reactor was smaller, 650 ms).

For comparison, in our previous study we investigated propene hydrogenation in a corresponding chip with sputtered Pt surface.[45] The reaction yield for the chip with 20 mm channel length was 28 % at room temperature and 22 % for the chip with 10 mm channels at 50 °C which are much lower values than for the Pt nanoparticle chips. The conditions in the experiments were not, however, exactly identical. The channel depth in the sputtered chips was 50 µm vs. 100 µm for the ALD nanoparticle chips. However, the sputtered catalyst was covering all four sides of the channels whereas in this study it covers only three sides. In addition, the travel (contact) time of gas through the sputtered chips was halved (Table 2). Nevertheless, the comparison of specific activities of Pt surface for the ALD nanoparticle and the sputtered chips show that in the latter case the activity is lower, which is also demonstrating the advantage of nanoparticles (Table 2). We note, however, that the detailed understanding of such difference is out of scope of this publication and will be addressed in our future studies.

Reaction yield for the chip with 20 mm channel length and 40 ALD cycles was monitored for four hours at 50 °C, while the reaction gas mixture was continuously flowing through the chip. During the course of the experiment, the yield decreased from 100 % to 50 % (Figure 6b). After an extended period, however, the reactor was completely deactivated. In batch type reactors, Pt nanoparticle catalysts have been shown to deactivate already in less than an hour.[53,54] Deactivation is likely due to the poisoning of catalyst surface by carbonaceous species as has been observed for other hydrocarbon hydrogenation reactions on different metal catalysts.[55,56] The catalyst activity for the samples with TiO_2 supports could not be regenerated by flushing with hydrogen at 50 °C, which was enough to recover catalyst activity on Piranha treated chips and on sputtered Pt film used in the previous study. The similarity of sputtered Pt and Piranha treated microreactors is, very likely, because in both cases we dealt with high surface coverage of Pt. Unfortunately, the laminate capping did not allow treatment at higher temperatures, which could be a possible solution for ALD nanoparticle microreactors to reactivate Pt. Therefore, the possibility to reactivate the 50 cycles Piranha treated chip is a significant advantage over TiO_2 chips.

We also tested the propene hydrogenation with parahydrogen-enriched H_2. The enrichment was achieved by flowing high-purity hydrogen gas through a copper tube packed with the ortho-para conversion

catalyst FeO(OH) immersed in liquid nitrogen (77 K) as explained in Ref. 39. It is well-known that the pairwise addition of both hydrogens of one parahydrogen molecule to magnetically inequivalent positions in a substrate molecule results in significantly enhanced NMR signals via parahydrogen-induced polarization (PHIP) effect, if the correlation of nuclear spins is preserved.[57–59] The effect has been observed in both homogeneous and heterogeneous hydrogenations over supported metal catalysts.[60–69] It has been shown in the literature that the pairwise addition selectivity is strongly dependent on the size of Pt metal nanoparticles and the type of the support, with smaller nanoparticles (< 1 nm)[61] and TiO_2 support providing strongest PHIP effect[65]. Powder-like catalysts prepared by impregnation method were used in those studies. Herein, some of our microreactors had quite similar properties of the catalyst, i.e. small Pt nanoparticle size and TiO_2 as a support layer, but the method of preparation was very different (ALD). At the same time, some of the microreactors provided a significant activity, for instance, ALD TiO_2 support with 20 cycles of Pt. In the experiments with parahydrogen, however, no PHIP was observed from any examined microreactors, implying that the pairwise addition selectivity was negligible. The reasons for this are not well-understood, but we stress the differences in preparation procedure of the nanoparticles and the support layer. One can expect different Pt surface defects formed by ALD and the impregnation method, and a different distribution of Pt crystal faces as well. In turn, this can be crucial for observation of the enhanced NMR signals as properties of Pt surface play a key role for PHIP observation.[65] Moreover, the influence of Pt support via metal-support interactions may be also very different, because in this study we did not use any reductive treatment with H_2, as it was not needed with ALD. As a common, metal-support interactions are revealed after the reductive treatment. Thus, in addition to significantly different Pt surface we may have no beneficial effect stem from TiO_2 support as well. In other words, the alteration of the preparation procedure may significantly diminish the concentration of catalytically active sites responsible for the pairwise addition, leading to the absence of PHIP. We believe, however, that further development of ALD method for catalysts deposition and microreactor technology will provide a better understanding of the problem. Another issue that may have an effect on the PHIP observation is the relatively low temperatures used in the experiments. The current chip construction does not allow rising the temperature. Meanwhile, the activation energies for pairwise and non-pairwise additions may be different, with higher values for the former one. The influence of temperature is, however, not very clear. For instance, no significant temperature influence on PHIP amplitude was observed for propyne hydrogenation over Pd nanoparticles,[70] whereas there are conference contributions describing that the temperature has a significant influence on propene

hydrogenation over Pt/TiO_2 and Ir/TiO_2.[71] The temperature issue certainly should be addressed in the context of ALD microreactors when the construction will be modified to allow high temperature studies.

Conclusions

This is, to the best of our knowledge, the first report of the fabrication and use of a metallic catalyst nanoparticles directly deposited into a microreactor by ALD. We have demonstrated that ALD can be used to deposit metal catalysts enabling high conversion rates. ALD of metals is more challenging than that of oxides, but they display the full benefits of ALD such as conformal deposition. ALD catalysts can be deposited in porous and highly 3D-channels, increasing solid-fluid interface significantly. Thermal ALD methods are easier to apply, but plasma-enhanced processes can be applied when extreme channel aspect ratios are not present. Plasma-enhanced deposition has been shown to work well for noble metals. Platinum was our first choice for catalyst, but ALD can be used to deposit various other noble metals also. Deposition of bimetallic particles allows even more degrees of freedom into catalyst design. Plethora of different oxides can also be deposited to act as support or active catalyst and the properties of these can be altered further by doping with different metals.

Wall-coated microreactors enable easy implementation of various schemes developed for catalyst design by ALD. Applying these methods may allow stabilization of catalysts against deactivation and provide enhanced activity and selectivity required for efficient operation.

We have observed differences in the poisoning and reactivation of Pt nanoparticles on TiO_2 versus Pt nanoparticles on Piranha treated silicon surface or continuous 100 nm thick sputtered Pt film. This needs to be studied further to understand the differences in these systems. A simple experiment would entail replacing the laminating foil with more temperature tolerant materials and using higher temperatures for catalyst reactivation.

Experimental Section

Microreactor fabrication

Microreactor channels were fabricated on silicon wafers using standard silicon microfabrication techniques followed by capping the channels with a laminating foil. Detailed description of the fabrication can be found in Supporting Information.

Catalyst preparation

Pt nanoparticles were deposited by ALD on two different supports, ALD TiO_2 or Piranha treated Si. Piranha treatment was done by dipping the microreactors into room temperature 4:1 H_2SO_4:H_2O_2 solution for 1 min. Picosun R-200 advanced remote plasma-enhanced ALD tool was used to deposit TiO_2 support and Pt nanoparticles. 50 nm of TiO_2 (850 cycles) was deposited thermally at 300 °C from $TiCl_4$ (≥99.0 %, Fluka Analytical) and H_2O using $TiCl_4$-N_2-H_2O-N_2 cycle sequence of 0.3-4-0.1-10 s. Both precursors were kept at 20 °C with Peltier cooling elements and vapor drawn from the precursor bottles. Pt was deposited using trimethyl-(methylcyclopentadienyl)-platinum(IV) ($MeCpPtMe_3$) (99 %, Strem Chemicals) and O_2-plasma. $MeCpPtMe_3$ was heated to 55 °C to achieve sufficient vapor pressure. $MeCpPtMe_3$ pulse length was 1.0 s followed by a 4.0 s purge. O_2-plasma pulse was 10.5 s consisting of 2 s flow stabilization prior to initiation of 2000 W RF power for 8 s followed by 0.5 s post plasma stabilization time. After the plasma pulse, the reactor was purged for 10 s. Carrier gas through plasma unit was argon whereas nitrogen was used as carrier gas for other precursors. Either 5, 10, 20, 40 or 50 cycles of Pt was deposited on the microreactors.

For particle size analysis 426 cycles of TiO_2 (target thickness 20 nm) was deposited on top of 50 nm thick Si_3N_4 TEM windows (Ted Pella, Inc.) followed by 5, 10, 20, 40 or 80 cycles of Pt. Tecnai F-20 transmission electron microscope (TEM) with beam energy of 200 kV was used for imaging. Fiji-image analysis software[72,73] was used to process images and calculate particle sizes. Image processing steps are shown in Supporting Information.

NMR characterization

^{1}H NMR spectra were measured with Bruker Avance III 300 spectrometer and RD NMR TOF images with Bruker DSX 300 spectrometer. Both spectrometers operate at 300 MHz proton resonance frequency. The same double-probe system was used in both spectrometers. Spatial encoding was carried out with a Bruker Micro 2.5 imaging probe, using an RF insert with a bird cage coil (inner diameter 25 mm and height 35 mm). The microfluidic reactors were centered inside the encoding coil with the help of a home-built chip holder made of Teflon (see Figure 1). A home-built detection probe was pushed inside the hollow interior of the imaging probe. The detection microsolenoid was wound around the 360 µm outlet capillary out of 120 µm thick copper wire. The length of the coil was 3 mm and it consisted of 18 loops. The coil was positioned ca. 10 mm below the lowest point of the encoding coil. Further details about RD NMR experiments can be found from Supporting Information.

Before the NMR experiments, propene and hydrogen gas were premixed in 1:3 ratio in a 1 L cylinder. The total absolute pressure of the mixture was about 5.7 bar. The mixture was allowed to settle for 20 to

30 min prior to the experiments. Then the gas mixture was released to flow through the microfluidic reactor to perform a continuous flow propene hydrogenation. The gas flow rate was controlled by a valve at the end of the flow system. The pressure in the microfluidic flow system was kept approximately equal to the pressure inside the gas cylinder. The hydrogenation reaction was performed either at room temperature or at slightly elevated temperature of about 50 °C, using a home-built air heating system. To ease the handling of the chips, they were glued on the top of a 1.4 mm glass plate before the NMR experiments in order to prevent the breakage of the chips.

The experimental conditions for Piranha treated chips with 50 cycles of Pt were slightly different: propene:H_2 ratio was 2:3 and the total absolute pressure was 7.5 bar.

In order to visualize mass transport, RD TOF NMR images of pure propene (4.3 bar) flowing through the reactor were measured as well.

Acknowledgements

V.-V.T. acknowledges the Academy of Finland for financial support (grant numbers 289649 and 294027). V.R. is grateful for funding by Finnish Cultural Foundation. A.S. thanks the Graduate School of Computational Chemistry and Molecular Spectroscopy (LASKEMO) for funding. Micronova Nanofabrication Centre of Aalto University is thanked for providing facilities for microreactor fabrication. V.V.Z. and I.V.K. thank RFBR (grant # 16-03-00407) for financial support.

Notes and references

[1] F. Zaera, *Catalysis Letters* **2012**, 142, 501.

[2] J. Zečević, G. Vanbutsele, K. P. de Jong, J. A. Martens, *Nature* **2015**, 528, 245.

[3] M. Valden, X. Lai, D. W. Goodman, *Science* **1998**, 281, 1647.

[4] J. Greeley, M. Mavrikakis, *Nat. Mater.* **2004**, 3, 810.

[5] K. F. Jensen, *Chem. Eng. Sci.* **2001**, 56, 293.

[6] B. Gutmann, D. Cantillo, C. O. Kappe, Angew. Chem. Int. Ed. **2015**, 54, 6688.

[7] B. J. O'Neill, D. H. K. Jackson, J. Lee, C. Canlas, P. C. Stair, C. L. Marshall, J. W. Elam, T. F. Kuech, J. A. Dumesic, G. W. Huber, *ACS Catal.* **2015**, 5, 1804.

[8] S. M. George, *Chem. Rev.* **2010**, 110, 111.

[9] V. Miikkulainen, M. Leskelä, M. Ritala, and R. L. Puurunen, *J. Appl. Phys.* **2013**, 113, 021301.

[10] M. Ritala, M. Leskelä, J.-P. Dekker, C. Mutsaers, P. J. Soininen, J. Skarp, Chem. Vap. Deposition **1999**, 5, 7.

[11] A. J. M. Mackus, M. J. Weber, N. F. W. Thissen, D. Garcia-Alonso, R. H. J. Vervuurt, S. Assali, A. A. Bol, M. A. Verheijen, W. M. M. Kessels, *Nanotechnology* **2016**, 27, 034001.

[12] M. J. Weber, A. J. M. Mackus, M. A. Verheijen, C. van der Marel, W. M. M. Kessels, *Chem. Mater.* **2012**, 24, 2973.

[13] E. Rikkinen, A. Santasalo-Aarnio, S. Airaksinen, M. Borghei, V. Viitanen, J. Sainio, E. I. Kauppinen, T. Kallio, A. O. I. Krause, *J. Phys. Chem. C* **2011**, 115, 23067.

[14] A. Santasalo-Aarnio, E. Sairanen, R. M. Arán-Ais, M. C. Figueiredo, J. Hua, J. M. Feliu, J. Lehtonen, R. Karinen, T. Kallio, *J. Catal.* **2014**, 309, 38.

[15] R. Beetstra, U. Lafont, J. Nijenhuis, E. M. Kelder, J. R. van Ommen, *Chem. Vap. Deposition* **2009**, 15, 227.

[16] W. Setthapun, W. D. Williams, S. M. Kim, H. Feng, J. W. Elam, F. A. Rabuffetti, K. R. Poeppelmeier, P. C. Stair, E. A. Stach, F. H. Ribeiro, J. T. Miller, C. L. Marshall, *J. Phys. Chem. C* **2010**, 114, 9758.

[17] J. Li, X. Liang, D. M. King, Y.-B. Jiang, A. W. Weimer, *Appl. Catal. B* **2010**, 97, 220.

[18] R. Karinen, S. Airaksinen, P. Kiviranta, K. Keskinen, J. Linnekoski, P. Uusi-Kyyny, A. O. I. Krause, *Top. Catal.* **2011**, 54, 1206.

[19] A. M. Armani, R. P. Kulkarni, S. E. Fraser, R. C. Flagan, K. J. Vahala, *Science* **2007**, 317, 783.

[20] V. Lien, F. Vollmer, *Lab chip* **2007**, 7, 1352.

[21] M. Zuborova, Z. Demianova, D. Kaniansky, M. Masar, and B. Stanislawski., *J. Chromatogr. A* **2003**, 990, 179.

[22] E. Hoffmann and V. Stroobant, *Mass Spectrometry: Principles and Application*, 3rd ed., Wiley, New York, **2007**.

[23] J. Wua, M. Gu, *J. Biomed Opt.* **2011**, 16, 080901.

[24] A. J. deMello, *Nature* **2006**, 442, 394.

[25] E. Harel, *Lab Chip* **2009**, 9, 17.

[26] B. Blümich, *NMR Imaging of Materials*, Oxford University Press, Oxford, **2000**.

[27] D. L. Olson, T. L. Peck, A. G. Webb, R. L. Magin, J. V. Sweedler, *Science* **1995**, 270, 1967.

[28] J. D. Trumbull, I. K. Glasgow, D. J. Beebe, R. L. Magin, *IEEE Transact. Biomed. Eng.* **2000**, 47, 3.

[29] H. Wensink, F. Benito-Lopez, D. C. Hermes, W. Verboom, H. J. G. E. Gardeniers, D. N. Reinhoudt, A. van den Berg. *Lab Chip* **2005**, 5, 280.

[30] S. Ahola, F. Casanova, J. Perlo, K. Münnemann, B. Blümich, S. Stapf, *Lab Chip* **2005**, 6, 90.

[31] S. Ahola, V.-V. Telkki, S. Stapf, *Lab Chip* **2012**, 12, 1823.

[32] R. M. Fratila, M. V. Gomez, S. Sýkora, A. H. Velders, *Nat. Commun.* **2014**, 5, 3025.

[33] J. Bart, A. J. Kolkman, A. J. Oosthoek-de Vries, K. Koch, P. J. Nieuwland, J. W. G. Janssen, P. J. M. van Bentum, K. A. M. Ampt, F. P. J. T. Rutjes, S. S. Wijmenga, J. G. E. Gardeniers, A. P. M. Kentgens, *J. Am. Chem. Soc.* **2009**, 131, 5014.

[34] K. C. H. Tijssen, J. Bart, R. M. Tiggelaar, J. W. G. Janssen, A. P. M. Kentgens, P. J. M. van Bentum, *J. Magn. Reson.* **2016**, 263, 136.

[35] G. Finch, A. Yilmaz, M. Utz, *J. Magn. Reson.* **2016**, 262, 73.

[36] C. Hilty, E. E. McDonnell, J. Granwehr, K. L. Pierce, S. Han, A. Pines, *P. Natl. Acad. Sci.* **2005**, 102, 14960.

[37] V.-V. Telkki, C. Hilty, S. Garcia, E. Harel, A. Pines, *J. Phys. Chem. B* **2007,** 111, 13929.

[38] V.-V. Telkki, V. V. Zhivonitko, S. Ahola, K. V. Kovtunov, J. Jokisaari, I. V. Koptyug, *Angew. Chem. Int. Ed.* **2010**, 49, 8363.

[39] V. V. Zhivonitko, V.-V. Telkki, I. V. Koptyug, *Angew. Chem. Int. Ed.* **2012**, 51, 8054.

[40] V.-V. Telkki, V. V. Zhivonitko, *J. Magn. Reson.* **2011**, 210, 238.

[41] L.-S. Bouchard, S. R. Burt, M. S. Anwar, K. V. Kovtunov, I. V. Koptyug, A. Pines, *Science* **2008**, 319, 442.

[42] R. Jiménez-Martínez, D. J. Kennedy, M. Rosenbluh, E. A. Donley, S. Knappe, S. J. Seltzer, H. L. Ring, V. S. Bajaj, J. Kitching, *Nat. Commun.* **2013**, 5, 3908.

[43] A. J. Moule, M. Spence, S. Han, J. Seeley, K. Pierce, S. Saxena, A. Pines, *Proc. Natl. Acad. Sci. U.S.A.* **2003**, 100, 9122.

[44] J. Granwehr, E. Harel, S. Han, S. Garcia, A. Pines, *Phys. Rev. Lett.* **2005**, 95, 075503.

[45] V. V. Zhivonitko, V.-V. Telkki, J. Leppäniemi, G. Scotti, S. Franssila and I. V. Koptyug, *Lab Chip*, **2013**, 13, 1554.

[46] E. Harel, C. Hilty, K. Koen, E. E. McDonnell, A. Pines, *Phys. Rev. Lett.* **2007**, 98, 017601.

[47] V. S. Bajaj, J. Paulsen, E. Harel, E., A. Pines, *Science* **2010**, 330, 1078.

[48] V.-V. Telkki, V. V. Zhivonitko, A. Selent, G. Scotti, J. Leppäniemi, S. Franssila, I. V. Koptyug, *Angew. Chem. Int. Ed.* **2014**, 53, 11289.

[49] J. Lu, K.-E. Low, Y. Lei, J. A. Libera, A. Nicholls, P. C. Stair, J. W. Elam, *Nat. Commun.*, **2014**, 5, 3264.

[50] M. J. Weber, M. A. Verheijen, A. A. Bol, W. M. M. Kessels, *Nanotechnology* **2015**, 26, 094002.

[51] L. Baker, A. S. Cavanagh, D. Seghete, S. M. George, A. J. M. Mackus, W. M. M. Kessels, Z. Y. Liu, F. T. Wagner, *J. Appl. Phys.* **2011**, 109, 084333.

[52] G. Cocco, R. Campostrini, M. A. Cabras, G. Carturan, *J. Mol. Catal.* **1994**, 94, 299.

[53] J. W. Yoo, D. Hathcock, M. A. El-Sayed, *J. Phys. Chem. A*, **2002**, 106, 2049.

[54] J. W. Yoo, D. Hathcock, M. A. El-Sayed, *J. Catal*. **2003**, 214, 1.

[55] G. Webb, *Cat. Today* **1990**, 7, 139.

[56] D. R. Kennedy, G. Webb, S. D. Jackson, D. Lennon, *Appl. Catal. A* **2004**, 259, 109.

[57] C. R. Bowers, D. P. Weitekamp, *J. Am. Chem. Soc.* **1987**, 109, 5541.

[58] C. R. Bowers, in *Encyclopedia of Nuclear Magnetic Resonance*, Vol. 9, Ed. D. M. Gant, R. K. Harris, Wiley, Chichester, **2002**, 750.

[59] S. B. Duckett, S. A. Colebrooke, in *Encyclopedia of Nuclear Magnetic Resonance*, Vol. 9, Ed. D. M. Gant, R. K. Harris, Wiley, Chichester, **2002**, 598.

[60] I. V. Koptyug, K. V. Kovtunov, S. R. Burt, M. S. Anwar, C. Hilty, S. I. Han, A. Pines and R. Z. Sagdeev, *J. Am. Chem. Soc.* **2007**, 129, 5580.

[61] K. V. Kovtunov, I. E. Beck, V. I. Bukhtiyarov, I. V. Koptyug, *Angew. Chem. Int. Ed.* **2008**, 47, 1492.

[62] A. M. Balu, S. B. Duckett and R. Luque, *Dalton Trans.* **2009**, 5074.

[63] K. V. Kovtunov, V. V. Zhivonitko, A. Corma and I. V. Koptyug, *J. Phys. Chem. Lett.* **2010**, 1, 1705.

[64] K. V. Kovtunov, V. V. Zhivonitko, L. Kiwi-Minsker, I.V. Koptyug, *Chem. Commun.* **2010**, 46, 5764.

[65] V. V. Zhivonitko, K. V. Kovtunov, I. E. Beck, A. B. Ayupov, V. I. Bukhtiyarov, I. V. Koptyug, *J. Phys. Chem. C* **2011**, 115, 13386.

[66] Q. X. Gong, J. Klankermayer and B. Blumich, *Chem. Eur. J.* **2011**, 17, 13795.

[67] R. Sharma, L. S. Bouchard, *Sci. Rep.* **2012**, 2, 277.

[68] S. Glöggler, A. M. Grunfeld, Y. N. Ertas, J. McCormick, S. Wagner, P. P. M. Schleker, L.-S. Bouchard, *Angew. Chem. Int. Ed.* **2015**, 54, 2452.

[69] R. Zhou, E. W. Zhao, W. Cheng, L. M. Neal, H. Zheng, R. E. Quiñones, H. E. Hagelin-Weaver, C. R. Bowers, *J. Am. Chem. Soc.* **2015**, 137, 1938.

[70] O. G. Salnikov, D. A. Barskiy, D. B. Burueva, Yu. K. Gulyaeva, B. S. Balzhinimaev, K. V. Kovtunov, I. V. Koptyug, *Appl. Magn. Reson.* **2014**, 45, 1051.

[71] R. Zhou, W. Cheng, L. M. Neal, H. E. Hagelin-Weaver, C. R. Bowers, AIChE annual meeting, San Francisco, 3–8 November **2013**, p. 583fq.

[72] J. Schindelin, I. Arganda-Carreras, E. Frise, V. Kaynig, M. Longair, T. Pietzsch, S. Preibisch, C. Rueden, S. Saalfed, B. Schmid, J.-Y. Tinevez, D. J. White, V. Hartenstein, K. Eliceiri, P. Tomancak, A. Cardona, Nat. Methods **2012**, 9, 676.

[73] C. A. Schneider, W. S. Rasband, K. W. Eliceiri, Nat. Methods **2012**, 9, 671.